Tris(*tert*-butoxy)siloxy Complexes as Single-Source Precursors to Homogeneous Zirconia- and Hafnia-Silica Materials. An Alternative to the Sol-Gel Method

Karl W. Terry, Claus G. Lugmair, and T. Don Tilley*

Contribution from the Department of Chemistry, University of California, Berkeley, Berkeley, California 94720-1460, and the Chemical Sciences Division, Lawrence Berkeley Laboratory, 1 Cyclotron Road, Berkeley, California 94720

Received May 2, 1997[⊗]

Abstract: The tris(*tert*-butoxy)siloxy complexes $M[OSi(O^tBu)_3]_4$ (**1**, M = Zr and **2**, M = Hf) are efficient single-source precursors to homogeneous zirconia-silica and hafnia-silica materials. The ceramic conversions occur pyrolytically at low temperatures, give the theoretical yield for $MO_2 \cdot 4SiO_2$ compositions, and occur without the incorporation of carbon. Compounds **1** and **2** are isomorphous, and crystallize as a mixture of two isomers. One isomer contains a 4-coordinate metal center, while the other is 5-coordinate and features a chelating η^2-$OSi(O^tBu)_3$ ligand. The solid-state transformation of **1** to $ZrO_2 \cdot 4SiO_2$ produces an open, fibrous material that is somewhat ordered with pores which are ∼20 nm in diameter. The solution-phase thermolysis of **1** produces a xerogel composed of small primary particles (≤∼5 nm). This xerogel possesses a high surface area (700 $m^2\ g^{-1}$ for samples heated to 200 °C). Solutions of the precursors have been used to cast crack-free thin films of $MO_2 \cdot 4SiO_2$. The $MO_2 \cdot 4SiO_2$ materials are amorphous as initially formed, and subsequent crystallizations of tetragonal ZrO_2, monoclinic ZrO_2, and cristobalite occur at relatively high temperatures. The enhanced stabilization of the amorphous and tetragonal phases of zirconia, relative to those derived from many sol-gel systems, implies that these single-source precursors initially produce homogeneous materials and that subsequent crystallizations are to a large degree diffusion-controlled. Homogeneity in the initially formed $ZrO_2 \cdot 4SiO_2$ material is also suggested by solid-state ^{29}Si NMR spectra. The molecular route to oxide materials described here represents an alternative to the sol-gel method and may offer certain advantages.

Introduction

The search for advanced materials with unique properties has increasingly focused on more intricate three-dimensional networks, which may involve complex stoichiometries (e.g., in ceramic superconductors such as $HgBa_2Ca_2Cu_3O_{8+\delta}$) or architectures (e.g., in zeolitic materials). Thus, development of synthetic strategies which allow precise control over the evolution of a solid-state structure, at the atomic level, has become an important goal in materials science.[1] A common approach employs molecular precursors, which offer fine control of stoichiometries, efficient incorporation of fundamental building blocks, and low-temperature, kinetically controlled pathways to metastable structures.[2]

Considerable attention has focused on oxide materials and their preparations by the sol-gel process.[3] This very powerful synthetic method, based on the hydrolysis/condensation of metal alkoxide precursors, provides reliable routes to pure metal oxides and composite materials which may be processed into a variety of forms (thin films, fibers, monoliths, etc.). One limitation of this method is its restriction to fairly polar media, as in aqueous or alcoholic solutions. Another potential problem concerns the inherent difficulty in obtaining homogeneous (atomically well-mixed) multicomponent oxides by the sol-gel method, since different metal alkoxide precursors hydrolyze at different rates, leading to homometallic M−O−M linkages and heterogeneous mixtures of oxides.[3,4]

We have been investigating an alternative route to mixed-element oxide materials, utilizing oxygen-rich "single-source precursor" molecules which possess the basic building blocks for forming the targeted oxide material.[5] This approach is based on initial findings that metal derivatives of $-OSi(O^tBu)_3$ cleanly eliminate isobutylene and water at remarkably low temperatures (100−150 °C) to form $M_xSi_yO_z$ materials. Simple tris(alkoxy)-

[⊗] Abstract published in *Advance ACS Abstracts,* September 15, 1997.

(1) (a) *Ultrastructure Processing of Ceramics, Glasses, and Composites*; Hench, L. L., Ulrich, D. R., Eds.; Wiley: New York, 1984. (b) *Ultrastructure Processing of Advanced Materials*; Uhlmann, D. R., Ulrich; D. R., Eds.; Wiley: New York, 1992. (c) *Better Ceramics Through Chemistry VI*; Cheetham, A. K., Brinker, C. J., Mecartney, M. L., Sanchez, C., Eds.; Materials Research Society Symposium Proceedings Vol. 360; Materials Research Society: Pittsburgh, 1994, and previous volumes in this series. (d) *Materials Chemistry - An Emerging Discipline*; Interrante, L. V., Casper, L. A., Ellis, A. B., Eds.; Advances in Chemistry Series 245; American Chemical Society: Washington, DC, 1992. (e) *Inorganic Materials*; Bruce, D. W., O'Hare, D., Eds.; Wiley: New York, 1992. (f) Stein, A.; Keller, S. W.; Mallouk, T. E. *Science* **1993**, *259*, 1558.

(2) Selected references on the single source precursor approach: (a) Cowley, A. H.; Jones, R. A. *Angew. Chem., Int. Ed. Engl.* **1989**, *28*, 1208. (b) Williams, A. G.; Interrante, L. V. In *Better Ceramics Through Chemistry*; Brinker, C. J., Clark, D. E., Ulrich, D. R., Eds.; Materials Research Society Symposia Proceedings Vol. 32; North-Holland: New York, 1984, p 152. (c) Apblett, A. W.; Warren, A. C.; Barron, A. R. *Chem. Mater.* **1992**, *4*, 167. (d) Chaput, F.; Lecomte, A.; Dauger, A.; Boilot, J. P. *Chem. Mater.* **1989**, *1*, 199. (e) Hoffman, D. M. *Polyhedron* **1994**, *13*, 1169. (f) Mehrotra, R. C. *J. Non-Cryst. Solids* **1990**, *121*, 1. (g) Hubert-Pfalzgraf, L. G. *New. J. Chem.* **1987**, *11*, 663. (h) Bradley, D. C. *Polyhedron* **1994**, *13*, 1111. (i) Chandler, C. D.; Roger, C.; Hampden-Smith, M. J. *Chem. Rev.* **1993**, *93*, 1205.

(3) (a) Brinker, C. J., Scherer, G. W. *Sol-Gel Science*; Academic Press: Boston, 1990. (b) *Sol-Gel Technology for Thin Films, Fibers, Preforms, Electronics, and Specialty Shapes*; Klein, L. C., Ed.; Noyes: Park Ridge, NJ, 1988. (c) Corriu, R. J. P.; Leclercq, D. *Angew. Chem., Int. Ed. Engl.* **1996**, *35*, 1421. (d) Guglielmi, M.; Carturan, G. *J. Non-Cryst. Solids* **1988**, *100*, 16. (e) Brinker, C. J. *J. Non-Cryst. Solids* **1988**, *100*, 31. (f) Schmidt, H. *J. Non-Cryst. Solids* **1988**, *100*, 51. (g) Sanchez, C.; Livage, J.; Henry, M.; Babonneau, F. *J. Non-Cryst. Solids* **1988**, *100*, 165.

(4) (a) Schubert, U. *J. Chem. Soc., Dalton Trans.* **1996**, 3343. (b) Schubert, U.; Hüsing, N.; Lorenz, A. *Chem. Mater.* **1995**, *7*, 2010. (c) Schmidt, H.; Scholze, H.; Kaiser, A. *J. Non-Cryst. Solids* **1982**, *48*, 65.

S0002-7863(97)01405-4 CCC: $14.00

siloxide complexes seem well suited as precursors to oxide materials, since the elements to be incorporated into the structure are initially bonded only to oxygen. This method can be used to obtain high surface area powders or thin films, and recently has been extended by others to the production of antireflective TiO_2-SiO_2 films by a CVD process.[6] These pyrolytic conversions are nonhydrolytic, in that they do not require added water for network formation. Thus, this precursor route is quite amenable to solution-phase conversions to networks and may be carried out in nonpolar solvents. Other nonhydrolytic methods which have been developed for synthesis of mixed-element oxides are based on condensations of metal alkoxides with metal acetates[7] and condensations of metal alkoxides with metal halides.[8]

In this paper, we describe conversions of the molecular precursors $M[OSi(O^tBu)_3]_4$ (**1**, M = Zr; **2**, M = Hf) to zirconia- and hafnia-silica materials. Zirconia-containing glasses have been heavily investigated as structural materials with low thermal expansions, high fracture toughness, and excellent resistance to chemical corrosion.[9] They are also attracting considerable attention as catalysts and catalyst supports.[10,11] Due to their refractory nature, these materials are difficult to shape into desired forms, and for this reason considerable attention has focused on sol-gel processing methods. However, it is difficult to obtain homogeneous ZrO_2-SiO_2 gels by this route, given the great difference in reactivity between alkoxides of silicon and zirconium.[12] This is a key issue since homogeneous gels, with a maximum number of Zr−O−Si heterolinkages, are thought to possess superior processing properties and lead to improved mechanical properties.[13] In addition, heterolinkages are associated with the presence of surface acid sites, which play an important role in catalysis.[14] To achieve greater homogeneity in the gels, several modified sol-gel procedures have been developed, including prehydrolysis of the silicon alkoxide[15] and retardation of the rate of hydrolysis for the zirconium component via incorporation of chelating ligands.[16] Here we show that **1** and **2** are good precursors to well-mixed zirconia- and hafnia-silica materials. The solid-state conversion of **1** to zirconia-silica results in ordered, porous structures.

Table 1. Selected Interatomic Distances (Å) and Angles (deg) for $Zr[OSi(O^tBu)_3]_4$ (**1**)

(a) Bond Distances			
Zr(1)−Si(1)	2.987(3)	Zr(1)−O(1)	2.038(6)
Zr(1)−O(2)	2.450(6)	Zr(1)−O(5)	1.956(6)
Zr(1)−O(9)	1.965(7)	Zr(1)−O(13)	1.955(7)
Zr(2)−O(17)	1.945(6)	Zr(2)−O(17)	1.945(6)
Zr(2)−O(21)	1.946(6)	Zr(2)−O(21)	1.946(6)
(b) Bond Angles			
O(1)−Zr(1)−O(5)	92.9(3)	O(1)−Zr(1)−O(2)	64.1(2)
O(1)−Zr(1)−O(13)	118.2(3)	O(1)−Zr(1)−O(9)	121.8(3)
O(2)−Zr(1)−O(9)	90.0(2)	O(2)−Zr(1)−O(5)	157.0(3)
O(5)−Zr(1)−O(9)	103.2(3)	O(2)−Zr(1)−O(13)	88.8(2)
O(9)−Zr(1)−O(13)	111.7(3)	O(5)−Zr(1)−O(13)	103.3(3)
O(17)−Zr(2)−O(21)	109.0(3)	O(17)−Zr(2)−O(17)	110.2(4)
O(17)−Zr(2)−O(21)	110.2(3)	O(17)−Zr(2)−O(21)	110.2(3)
O(21)−Zr(2)−O(21)	108.2(4)	O(17)−Zr(2)−O(21)	109.0(3)
Zr(1)−O(1)−Si(1)	109.9(3)	Zr(1)−O(2)−Si(1)	91.0(3)
Zr(1)−O(5)−Si(4)	170.0(5)	Zr(1)−O(9)−Si(2)	173.7(4)
Zr(1)−O(13)−Si(3)	179.7(4)	Zr(2)−O(17)−Si(6)	165.4(4)
Zr(2)−O(21)−Si(5)	167.8(4)		

Results

Synthesis and Characterization of the Molecular Precursors $M[OSi(O^tBu)_3]_4$ (M = Zr, Hf). The group 4 tris(*tert*-butoxy)siloxy complexes are best prepared by addition of 4 equiv of $HOSi(O^tBu)_3$[17] to the appropriate tetraamide $M(NEt_2)_4$[18] (eq 1). The resulting products are isolated from cold (−35 °C)

$$M(NEt_2)_4 + 4HOSi(O^tBu)_3 \xrightarrow{\text{pentane}} M[OSi(O^tBu)_3)_4 + 4HNEt_2 \quad (1)$$

1: M = Zr
2: M = Hf

pentane as colorless crystals, which fracture over the course of a few hours at room temperature. Compounds **1** and **2** exist as monomers in the solid-state (vide infra), but whereas **2** was found to be monomeric in benzene solution, **1** is dimeric in that solvent (by vapor diffusion). Variable-temperature ^1H NMR spectroscopy (toluene-d_8) indicated that there are no structural changes for **1** down to −80 °C. As expected, the ^{29}Si NMR resonances for these compounds appear at very high field (−100.50 ppm for **1** and at −97.06 ppm for **2**). In addition, these complexes exhibit strong infrared absorptions that may be attributed to the M−O−Si linkages,[19] at 935 (**1**) and 954 (**2**) cm^{-1}.

For comparison, the related siloxide complexes $M[OSiPh(O^tBu)_2]_4$ (**3**, M = Zr; **4**, M = Hf) were synthesized by silanolysis of the appropriate metal diethylamide. Compounds **3** and **4** are extremely soluble and precipitate slowly as opaque white powders from cold, saturated solutions. The first crop of crystals of **3** from pentane were characterized as the diethylamine adduct **3**·$HNEt_2$ (31% yield). A second crop gave a 14% yield of the base-free complex **3**. In contrast, the base-free hafnium derivative **4** was isolated in 68% yield as a single crop of crystals at −78 °C.

Single-Crystal X-ray Structures of 1 and 2. Crystals of **1** and **2** are isomorphous. Important bond distances and angles are listed in Tables 1 and 2. The unit cell (Figure 1) is quite large (23.8 × 13.3 × 62.2 Å for **1**) and contains molecules with two different coordination geometries (Figure 2). The

(5) (a) Terry, K. W.; Tilley, T. D. *Chem. Mater.* **1991**, *3*, 1001. (b) Terry, K. W.; Gantzel, P. K.; Tilley, T. D. *Chem. Mater.* **1992**, *4*, 1290. (c) Terry, K. W.; Gantzel, P. K.; Tilley, T. D. *Inorg. Chem.* **1993**, *32*, 5402 (d) Terry, K. W.; Lugmair, C. G.; Gantzel, P. K.; Tilley, T. D. *Chem. Mater.* **1996**, *8*, 274. (e) Lugmair, C. G.; Tilley, T. D.; Rheingold, A. L. *Chem. Mater.* **1997**, *9*, 339. (f) Su, K.; Tilley, T. D. *Chem. Mater.* **1997**, *9*, 588. (g) Su, K.; Tilley, T. D.; Sailor, M. J. *J. Am. Chem. Soc.* **1996**, *118*, 3459.

(6) Narula, C. K.; Varshney, A.; Riaz, U. *Chem. Vap. Deposition* **1996**, *2*, 13.

(7) Jansen, M.; Guenther, E. *Chem. Mater.* **1995**, *7*, 2110.

(8) Andrianainarivelo, M.; Corriu, R.; Leclerq, D.; Mutin, P. H.; Vioux, A. *J. Mater. Chem.* **1996**, *6*, 1665.

(9) (a) Simhan, R. G. *J. Non-Cryst. Solids* **1983**, *54*, 335. (b) Yoldas, B. E. *J. Non-Cryst. Solids* **1980**, *38*−39, 81. (c) Paul, A. *J. Mater. Sci.* **1977**, *12*, 2246.

(10) (a) Soled, S.; McVicker, G. B. *Catal. Today* **1992**, *14*, 189. (b) Niwa, M.; Katada, N.; Murakami, Y. *J. Catal.* **1992**, *134*, 340. (c) Bosman, H. J. M.; Kruissink, E. C.; van der Spoel, J.; van den Brink, F. *J. Catal.* **1994**, *148*, 660. (d) Sohn, J. R.; Jang, H. J. *J. Mol. Catal.* **1991**, *64*, 349.

(11) (a) Miller, J. B.; Rankin, S. E.; Ko, E. I. *J. Catal.* **1994**, *148*, 673. (b) Miller, J. B.; Ko, E. I. *J. Catal.* **1996**, *159*, 58.

(12) Guizard, C.; Cygankiewicz, N.; Larbot, A.; Cot, L. *J. Non-Cryst. Solids* **1986**, *82*, 86.

(13) (a) Abe, Y.; Sugimoto, N.; Nagao, Y.; Misono, T. *J. Non-Cryst. Solids* **1989**, *108*, 150. (b) Nagarajan, V. S.; Rao, K. J. *J. Mater. Sci.* **1989**, *24*, 2140. (c) Nogami, M.; Tomozawa, M. *J. Am. Ceram. Soc.* **1986**, *69*, 99. (d) Nogami, M.; Nagasaka, K. *J. Non-Cryst. Solids* **1989**, *109*, 79.

(14) (a) Tanabe, K.; Sumiyoshi, T.; Shibata, K.; Kiyoura, T.; Kitagawa, J. *Bull. Chem. Soc. Jpn.* **1974**, *47*, 1064. (b) Miller, J. B.; Johnston, S. T.; Ko, E. I. *J. Catal.* **1994**, *150*, 311.

(15) (a) Miller, J. B.; Ko, E. I. *J. Catal.* **1995**, *153*, 194. (b) Monros, G.; Marti, M. C.; Carda, J.; Tena, M. A.; Escribano, P.; Anglada, M. *J. Mater. Sci.* **1993**, *28*, 5852. (c) Nogami, M. *J. Non-Cryst. Solids* **1985**, *69*, 415.

(16) (a) Toba, M.; Mizukami, F.; Niwa, S.; Sano, T.; Maeda, K.; Annila, A.; Komppa, V. *J. Mol. Catal.* **1994**, *94*, 85. (b) Salvado, I. M. M.; Serna, C. J.; Navarro, J. M. F. *J. Non-Cryst. Solids* **1988**, *100*, 330.

(17) Abe, Y.; Kijima, I. *Bull. Chem. Soc. Jpn.* **1969**, *42*, 1118.

(18) Bradley, D. C.; Thomas, I. M. *J. Chem. Soc.* **1960**, 3857.

(19) Hrncir, D. C.; Skiles, G. D. *J. Mater. Res.* **1988**, *3*, 410.

Table 2. Selected Interatomic Distances (Å) and Angles (deg) for $Hf[OSi(O^tBu)_3]_4$ (**2**)

(a) Bond Distances			
Hf(1)−Si(1)	2.967(2)	Hf(1)−O(1)	2.021(4)
Hf(1)−O(2)	2.419(4)	Hf(1)−O(5)	1.935(4)
Hf(1)−O(9)	1.949(4)	Hf(1)−O(13)	1.941(4)
Hf(2)−O(17)	1.912(4)	Hf(2)−O(17)	1.912(4)
Hf(2)−O(21)	1.929(4)	Hf(2)−O(21)	1.929(4)
(b) Bond Angles			
O(1)−Hf(1)−O(5)	92.4(2)	O(1)−Hf(1)−O(2)	64.9(1)
O(1)−Hf(1)−O(13)	118.9(2)	O(1)−Hf(1)−O(9)	121.8(2)
O(2)−Hf(1)−O(9)	90.0(1)	O(2)−Hf(1)−O(5)	157.3(2)
O(5)−Hf(1)−O(9)	102.5(2)	O(2)−Hf(1)−O(13)	89.2(2)
O(9)−Hf(1)−O(13)	111.7(2)	O(5)−Hf(1)−O(13)	103.3(2)
O(17)−Hf(2)−O(21)	108.9(2)	O(17)−Hf(2)−O(17)	110.0(2)
O(17)−Hf(2)−O(21)	110.0(2)	O(17)−Hf(2)−O(21)	110.0(2)
O(21)−Hf(2)−O(21)	109.0(3)	O(17)−Hf(2)−O(21)	108.9(2)
Hf(1)−O(1)−Si(1)	109.1(2)	Hf(1)−O(2)−Si(1)	91.3(2)
Hf(1)−O(5)−Si(4)	170.4(3)	Hf(1)−O(9)−Si(2)	174.3(3)
Hf(1)−O(13)−Si(3)	179.5(3)	Hf(2)−O(17)−Si(6)	165.5(3)
Hf(2)−O(21)−Si(5)	167.1(3)		

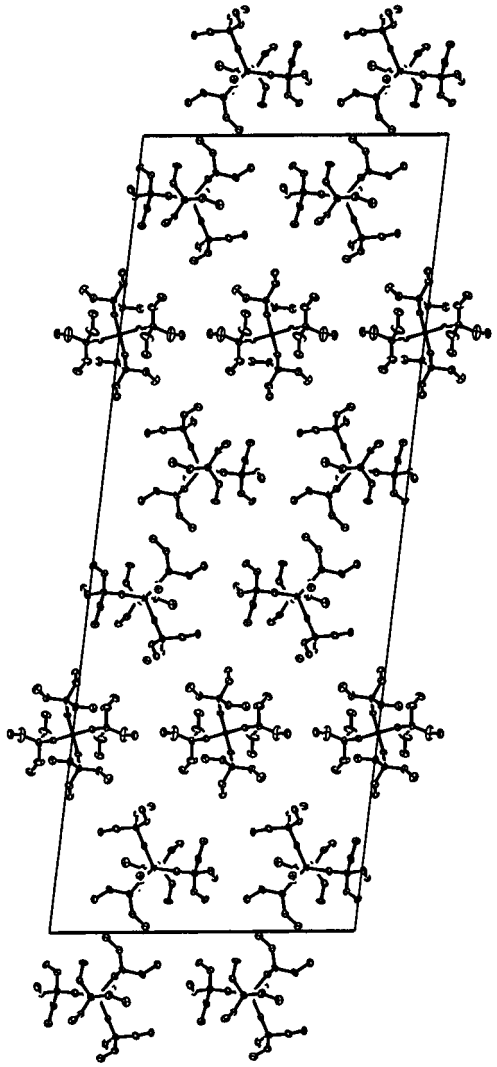

Figure 1. Unit cell of **1** viewed down the *b* direction.

asymmetric unit contains 1.5 formula units, as the 4-coordinate complexes lie on a 2-fold axis. The complete molecule in the asymmetric unit contains a 5-coordinate metal atom ligated by one bidentate and three monodentate $-OSi(O^tBu)_3$ ligands. The latter complex possesses an approximate trigonal-bipyramidal geometry, which is distorted by the presence of the chelate ring which imposes an O−Zr−O bond angle of only 64.1(2)° (64.9-(1)° for **2**). The pseudoequatorial atoms O(1), O(9), and O(13), and the Zr atom, are nearly planar (deviations from the least-squares plane are 0.32, 0.30, 0.30, and −0.03 Å, respectively). However, the O(13)−Zr(1)−O(9) angle of 111.7(3)° deviates considerably from 120°, and the O(2)−Zr(1)−O(5) angle is only 157.0(3)°. Presumably, constriction of the O(13)−Zr(1)−O(9) angle to 111.7(3)° results from the steric demands of the chelating siloxide ligand.

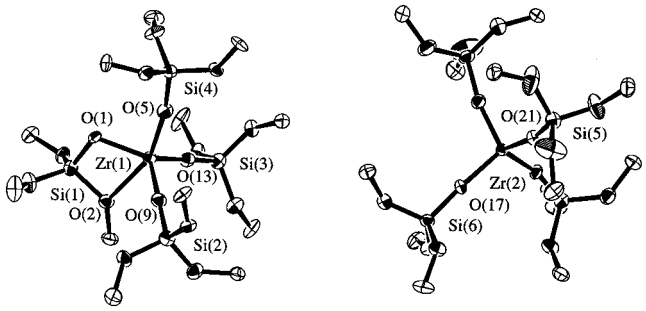

Figure 2. ORTEP view of the two structural isomers of **1.** Methyl groups have been removed for clarity.

Coordination of a $-O^tBu$ group in the bidentate siloxide ligand results in relatively long metal−oxygen distances which are consistent with dative bonds [Zr(1)−O(2), 2.450(6) Å; Hf-(1)−O(2), 2.419(4) Å].[20] As expected, this distance is significantly longer than the other metal−oxygen distance involving the bidentate ligand [Zr(1)−O(1), 2.038(6) Å; Hf(1)−O(1), 2.021(4) Å]. The metal−oxygen bond distances for the monodentate siloxide ligands range from 1.955(7) to 1.965(7) Å in **1**, and from 1.935(4) to 1.949(4) Å in **2**. For comparison, the metal−oxygen bond distances in the tetrahedral complexes range from 1.945(6) to 1.946(6) Å in **1**, and from 1.912(4) to 1.929(4) Å in **2**. The chelate rings in compounds **1** and **2** are both planar. The M−O(1)−Si(1) bond angles in the chelate ring are 109.9(3)° in **1** and 109.1(2)° in **2**, whereas the M−O(2)−Si(1) bond angles are 91.0(3)° in **1** and 91.3(2)° in **2**. As expected, the O−Si−O bond angles within the chelate rings (**1**, 94.9(3)°; **2**, 94.6(2)°) are much smaller than the other O−Si−O angles observed in these structures, which range from 105° to 115°. For the tetrahedral complexes, the M−O−Si bond angles range from 165.4(4)° to 167.8(4)° for **1** and from 165.5-(3)° to 167.1(3)° for **2**. The M−O−Si bond angles for the monodentate ligands in the 5-coordinate complexes range from 170.0(5)° to 179.7(4)° for **1** and from 170.4(3)° to 179.5(3)° for **2**. Note that the greater M−O−Si angles for the 5-coordinate (vs 4-coordinate) complexes are not accompanied by shorter M−O distances, which might have implied a higher bond order and a greater degree of $p_\pi-d_\pi$ donation.[21]

Pyrolytic Conversions of 1 and 2 to Silicate Materials. Compounds **1** and **2** are thermally labile, as shown by thermal gravimetric analysis (TGA). The TGA trace for **1** (Figure 3) shows a precipitous weight loss corresponding to a very clean ceramic conversion. The TGA curves for **1** and **2** are nearly identical, and at a heating rate of 2 °C min^{-1}, thermal decompositions of **1** and **2** exhibit remarkably low onset temperatures of 137 and 141 °C, respectively. Minimal dehydration continues slowly thereafter, until a constant weight corresponding to quantitative formation of $MO_2 \cdot 4SiO_2$ is established. For both compounds, no melting or sublimation was observed prior to thermolysis. Differential thermal analysis

(20) (a) Babaian, E. A.; Hrncir, D. C.; Bott, S. G.; Atwood, J. L. *Inorg. Chem.* **1986**, *25*, 4818. (b) Thewalt, U.; Lasser, W. *J. Organomet. Chem.* **1984**, *276*, 341.

(21) Fink, W. H.; Power, P. P.; Allen, T. L. *Inorg. Chem.* **1997**, *36*, 1431.

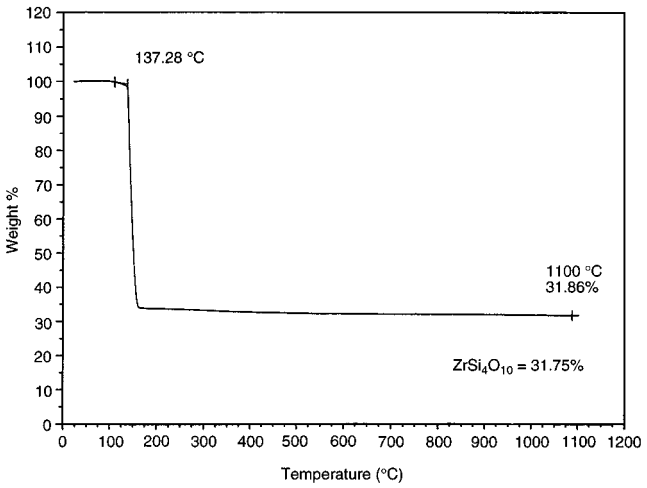

Figure 3. TGA trace for **1** under Ar, with a heating rate of 10 °C min^{-1}.

(DTA) traces for **1** and **2** contained endotherms for the decomposition, but none for melting. A sample of **1** pyrolyzed under oxygen at 200 °C contained only 0.57% carbon and 1.32% hydrogen (by combustion analysis), and these levels are reduced to <0.2 and 0.2%, respectively, after heating further to 500 °C. The volatile decomposition products from the thermolysis of **1** at 190−200 °C (after 5 min) were collected by vacuum transfer and identified by ^{1}H NMR spectroscopy as isobutene (11.7 equiv), water (5.4 equiv), and a slight trace of *tert*-butyl alcohol. The stoichiometry is therefore closely approximated by eq 2.

$$Zr[OSi(O^tBu)_3]_4 \xrightarrow[10^{-3}\ mmHg]{190-200\ °C} ZrO_2{\cdot}4SiO_2 + 12CH_2{=}CMe_2 + 6H_2O \quad (2)$$

Crystallizations and phase transformations were followed by X-ray powder diffraction (XRD), differential thermal analysis (DTA), infrared spectroscopy, and electron microscopy. Samples of **1** and **2** were initially heated at 400 °C for 2 h under oxygen or argon. These samples were then gradually taken to higher temperatures (900−1400 °C). The samples were heated at a given temperature for 2 h, and then cooled back to room temperature for analysis. The XRD powder patterns for samples resulting from thermolysis of **1** and **2** under oxygen and argon are shown in Figure 4. This data is also summarized in Table 3.

Interestingly, crystals of **1** retain their shape and morphology (in going from transparent to opaque) after decomposition at 1200 °C in air, with very little shrinkage (≤10%). A DTA curve for **1** under oxygen reveals a broad exotherm from 1150 to 1400 °C, which may be assigned to the crystallization of t-ZrO_2 (tetragonal zirconia). As shown in Figure 4a, samples of **1** heated under oxygen are amorphous to ∼1200 °C, where nanocrystalline t-ZrO_2 particles are first observed (average diameter 6 nm, as estimated by the Scherer equation[22]). Heating this sample at 1300 °C under argon led to growth of the t-ZrO_2 particles, and formation of detectable quantities of m-ZrO_2 (monoclinic zirconia). After further heating at 1400 °C, the average particle sizes for t-ZrO_2 and m-ZrO_2 were 28 and 29 nm, respectively, and the volume fraction of m-ZrO_2 relative to the total amount of crystalline ZrO_2 was 0.17.[23]

The crystallization of zirconia particles was also followed by infrared spectroscopy, which revealed the appearance of a broad absorption band at 600 cm^{-1} as the t-ZrO_2 particles formed, followed by a band at 742 cm^{-1}, attributed to m-ZrO_2.[24] These results confirmed what was determined from the XRD experiments, with respect to the temperatures of crystallization.

The material obtained by thermolysis of **1** at 200 °C under oxygen has a surface area of 118 $m^2\ g^{-1}$ and a pore volume of 0.84 $cm^3\ g^{-1}$ (BET method). Approximately 70% of the total surface area and 6% of the total pore volume may be attributed to pores with diameters between 15 and 30 Å. This material exhibits a type II isotherm, which indicates that 51% of the pore volume arises from macropores with diameters between 500 and 2000 Å. Analysis by transmission electron microscopy (TEM) revealed a relatively ordered, mesostructured material consisting of very thin fibers (∼20−50 Å thick), oriented roughly along the same direction (Figure 5a). Very similar structures are obtained for thermolyses under oxygen and nitrogen. Thermolysis at 400 °C gave a surface area of 118 $m^2\ g^{-1}$, which was reduced by further heating to 800 °C (82 $m^2\ g^{-1}$) and then 1200 °C (36 $m^2\ g^{-1}$; see Figure 6). Transmission electron micrographs of samples of **1** taken to 900 °C under oxygen also reveal a somewhat ordered, fibrous structure (Figure 5b). After heating to 1200 °C, partial sintering of the amorphous matrix (containing 6 nm t-ZrO_2 particles) to a porous vermicular structure is observed (Figure 5c), and samples taken to 1400 °C possess a sintered structure consisting of a densified silica matrix containing spherical ZrO_2 crystallites (Figure 5d). In contrast, materials obtained by thermolysis of **2** appear as agglomerates of small particles (8−32 nm at 400 °C), which slowly sinter as the temperature is increased to 1460 °C.

Thermolysis and heating of **1** under argon led to an earlier crystallization of t-ZrO_2 (at 1000 °C; see Figure 4b), and observation of m-ZrO_2 at 1300 °C. The sample heated to 1400 °C under argon contained t-ZrO_2 and m-ZrO_2 with particle sizes of 26 nm and 29 nm, respectively, and the volume fraction of m-ZrO_2 was 0.15. Whereas the materials obtained by heating **1** and **2** to 400 °C under oxygen are off-white powders, thermolysis under argon at 400 °C for 2 h produced black powders. An electron paramagnetic resonance spectrum of the black material obtained from the thermolysis of **1** gave a 1-electron g value of 2.0025 (g_{DPPH} = 2.0037), which may be attributed to surface oxygen vacancies (F centers) in zirconia nanoparticles.[25] Under argon, a heat treatment at 1100 °C for 2 h was required to render these materials completely white.

Whereas the thermolysis chemistry of **1** and **2** appears to be quite similar, there are significant differences in the solid-state phases that are generated. Thermolysis of **2** under both oxygen and argon produced c/t-HfO_2 (cubic or tetragonal hafnia) by 1000 °C (by XRD; Figure 4c,d). After this thermolysis, the HfO_2 crystallite sizes were too small to be estimated by XRD, and the XRD peaks were too broad to allow exact determination of the symmetry. Heating at 1200 °C under oxygen produced c/t-HfO_2 crystallites which were estimated to have an average diameter of approximately 6 nm (by XRD). Further heating of this sample to 1300 °C under argon resulted in crystallization of m-HfO_2, and heating to 1400 °C under argon yielded a mixture of c/t-HfO_2 (21 nm) and m-HfO_2 (27 nm) particles, with a volume fraction of 50% for each (by XRD). This sample also contained cristobalite, and there are very low intensity peaks at d = 4.43 and 3.29 Å which may be attributed to the presence of hafnon, $HfSiO_4$ (Figure 4c). In contrast, we found no evidence for the formation of zircon ($ZrSiO_4$) in the thermolysis

(22) Scherrer, P. *Nachr. Ges. Wiss. Göttingen* **1918**, 96.
(23) (a) Toraya, H.; Yoshimura, M.; Sõmiya, S. *J. Am. Ceram. Soc.* **1984**, *67*, C-119. (b) Ward, D. A.; Ko, E. I. *Chem. Mater.* **1993**, *5*, 956.
(24) McDevitt, N. T.; Baun, W. L. *Spectrochim. Acta* **1964**, *20*, 799.
(25) Liu, H.; Feng, L.; Zhang, X.; Xue, Q. *J. Phys. Chem.* **1995**, *99*, 332.

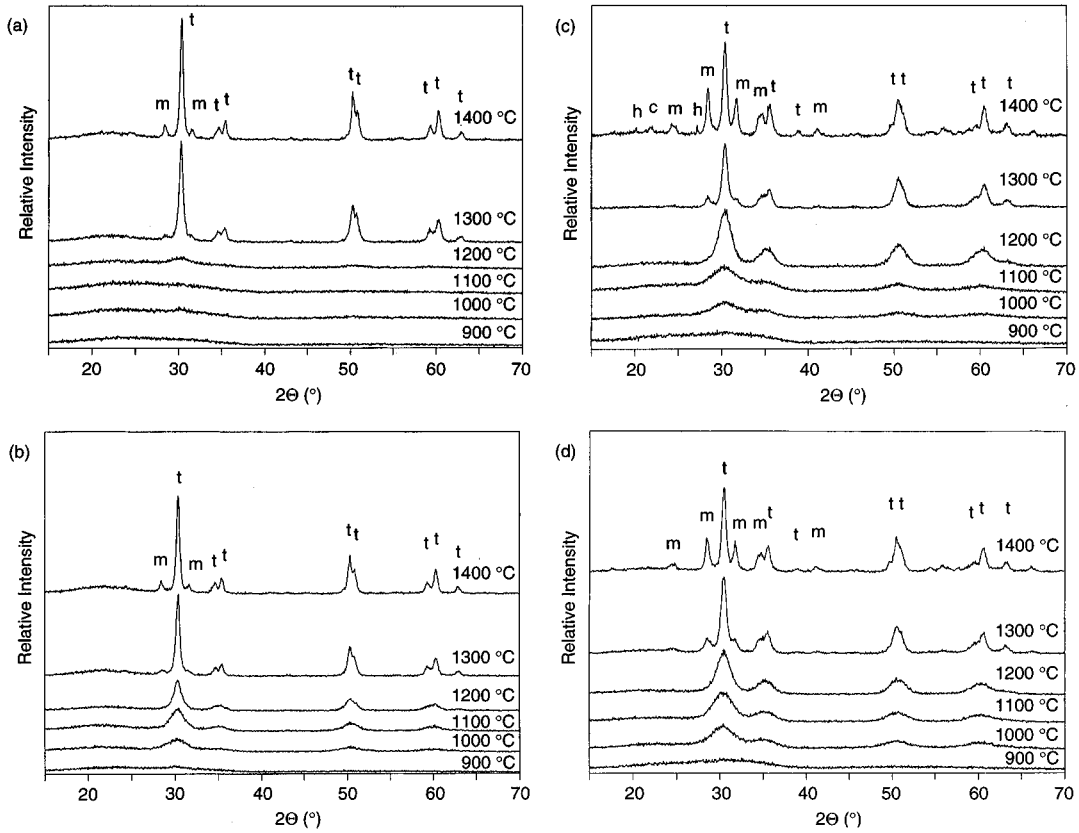

Figure 4. Room temperature XRD powder patterns of the materials obtained by thermolysis of **1** and **2** in the solid state at various temperatures: (a) **1** calcined under O_2, (b) **1** calcined under Ar, (c) **2** calcined under O_2, and (d) **2** calcined under Ar. (Key: m, monoclinic; t, tetragonal; c, cristobalite; h, hafnon.)

Table 3. Summary of Crystallization Behavior for Various Precursors

	precursor				
	1	**1**	**2**	**2**	xerogel (**1**)
atmosphere	Ar	O_2	Ar	O_2	O_2
lowest *T* t-MO_2 obsvd (XRD) (°C)	1000	1200	1000	1000	1000
lowest *T* m-MO_2 obsvd (XRD) (°C)	1300	1300	1300	1300	>1400
vol frac of m-MO_2 at 1400 °C	0.15	0.17	0.44	0.50	0.00
av particle diam (nm) at 1400 °C (for t-MO_2/m-MO_2)[a]	26/29	28/29	19/22	21/27	24/-
color	dark gray	white	dark gray	white	white

[a] By XRD.

of **1**. For comparison, a sample of **2** heated under argon exhibited the same crystallization behavior, but gave somewhat smaller crystallites (average diameters for c/t-HfO_2 and m-HfO_2 were 19 and 22 nm, respectively, at 1400 °C) and a volume fraction of 0.44 for m-HfO_2. The crystallization of t-HfO_2 was also signaled by the appearance of an infrared band at 600 cm^{-1} (at 1000 °C under O_2 or Ar), and calcination to 1300 °C resulted in appearance of three bands at 558, 643, and 751 cm^{-1}, which correspond to m-HfO_2.[24] TEM analysis of the materials obtained from **2** revealed the presence of denser, less featured, and more highly sintered particles relative to those from **1**.

Solid-State Thermolyses of 3 and 4. The TGA curves for compounds **3** and **4** under oxygen are similar. The onset temperatures for weight loss occur between 135−140 °C, but conversion to the final ceramic material occurs over a rather broad temperature range. The yields of the resulting $MO_2 \cdot 4SiO_2$ materials are 30.78% (for base free **3**) and 33.81% (for **4**), which can be compared to the theoretical yields of 31.32 and 36.12%, respectively. The more gradual weight losses, which occur over the temperature range 200−500 °C, most likely correspond to oxidation of the phenyl groups.

Synthesis of $MO_2 \cdot 4SiO_2$ Xerogels from Solution. The low-temperature thermolyses for **1** and **2** allow for the convenient use of these pyrolytic elimination reactions for forming silicate networks in solution. Thus, this process offers the novel opportunity for forming oxide networks *from nonpolar media*.

Typically, a solution of the precursor (**1** or **2**) is heated in a nonpolar solvent (e.g., benzene, toluene, xylenes, mesitylene) until a sudden, vigorous evolution of gas occurs to give a viscous gel. Gel solutions produced in toluene are transparent and colorless. Heating a solution of **1** in toluene (0.13 M) at 140 °C for 48 h in a sealed ampule produced a transparent monolith, which cracked only slightly upon air-drying over 5 days. A TEM micrograph of this material revealed a finely textured structure composed of very small particles (< 5 nm). The xerogel fragments were ground to a fine powder and then dried further under vacuum at 100 °C (12 h). TGA analyses of these gels reveal weight loss (up to ∼25%, depending upon the degree of "predrying") to ∼1150 °C, attributed to dehydration and further condensation of the network. Analysis of the gels by DTA did not reveal an exotherm corresponding to the crystallization of zirconia, presumably because this occurs slowly over a broad temperature range (vide infra).

The dried gel described above was calcined to higher temperatures in a tube furnace under flowing oxygen. The samples were heated at each temperature for 2 h, and then cooled

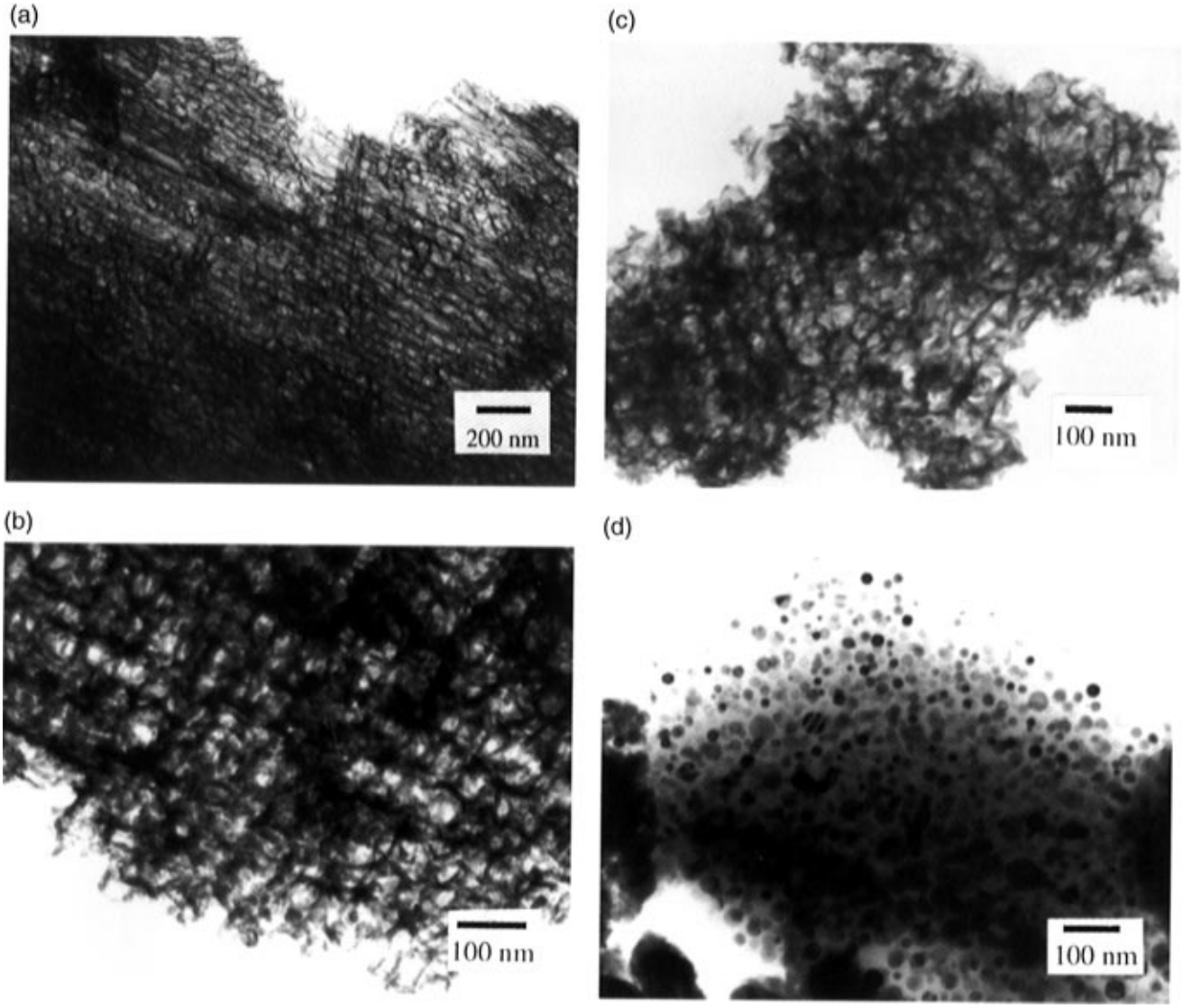

Figure 5. TEM photographs of materials obtained by thermolysis of **1** in the solid state under O_2 at (a) 200 °C, (b) 900 °C, (c) 1200 °C, and (d) 1400 °C.

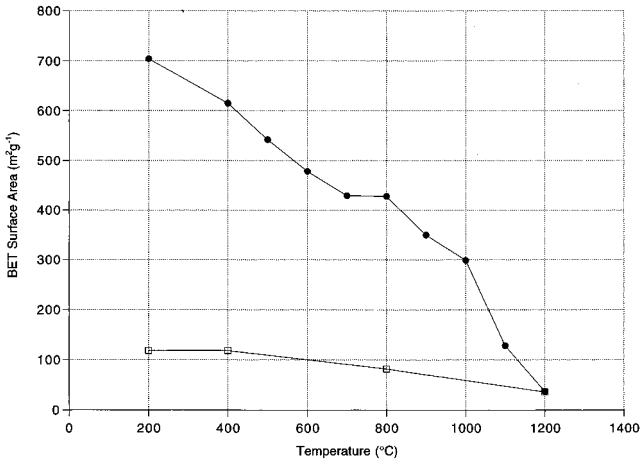

Figure 6. BET surface area as a function of calcination temperature for both the xerogel (filled circles) and the solid-state thermolysis product (open squares).

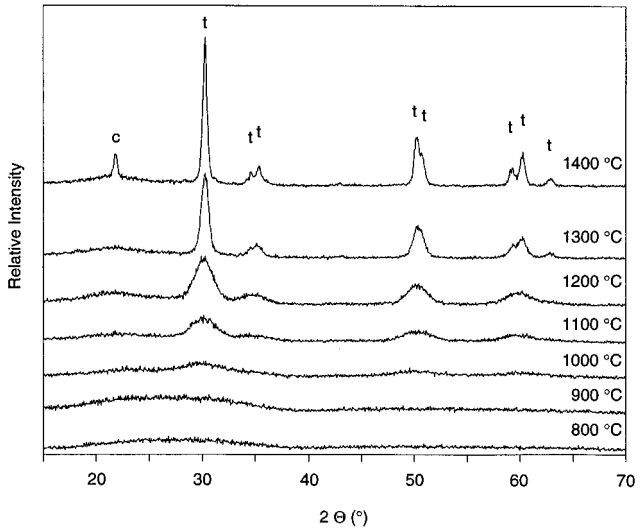

Figure 7. Room-temperature XRD powder patterns of xerogels derived from **1** calcined under O_2 to various temperatures. (Key: t, tetragonal; c, cristobalite).

to room temperature for analysis by XRD, FTIR spectroscopy, BET surface area analysis, ^{29}Si NMR spectroscopy, and TEM. Tetragonal ZrO_2 can first be detected by XRD after heating the sample to 1000 °C (Figure 7). Calcination to 1200 °C increased the crystallinity of the t-ZrO_2 phase and resulted in an average particle size of 5.3 nm. Heating to 1400 °C increased the average t-ZrO_2 particle size to 24 nm, but gave no detectable m-ZrO_2. Cristobalite, with an average crystallite size of 30 nm,

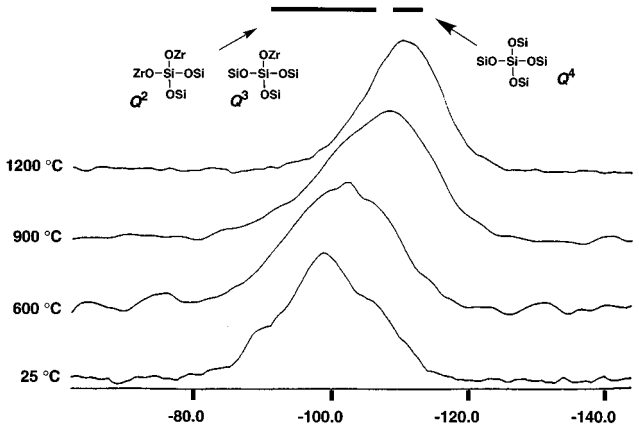

Figure 8. ^{29}Si MAS-NMR spectra of xerogels derived from **1** in refluxing xylenes, after calcination to various temperatures.

is also detected in this sample (by XRD). This crystallization behavior was substantiated by FTIR measurements, which revealed the crystallization of t-ZrO_2, but no detectable m-ZrO_2, over the temperature range 1000−1400 °C.

Figure 8 shows ^{29}Si MAS-NMR spectra for xerogels obtained from **1** which had been taken to various temperatures. The uncalcined gel gives rise to a broad envelope of resonances centered at −99 ppm, and heating to higher temperatures results in progressive shifts to higher field as $Si(OSi)_n(OZr)_m$ sites are replaced by $Si(OSi)_4$ sites.[7,8,26]

Figure 9 shows TEM micrographs of the xerogel material calcined at 900, 1200, and 1400 °C. The material taken to 900 °C has a granular appearance that is very similar to that of the uncalcined gel. The material calcined to 1200 °C consists of a smooth silica matrix containing spherical ZrO_2 particles (Figure 9b). As shown in Figure 9c, heating to 1400 °C produces larger zirconia nanoparticles with a greater dispersity in size.

A plot of the surface area vs calcination temperature (Figure 6) shows that a relatively high surface area (∼700 $m^2\ g^{-1}$) is observed for material heated to 200 °C. Further heat treatment results in a gradual reduction in the surface area. The xerogel calcined to 500 °C has a surface area of 542 $m^2\ g^{-1}$ and a total pore volume of 0.767 $cm^3\ g^{-1}$. Figure 10 shows the pore size distribution as calculated from the adsorption isotherm. The pore size distribution is fairly broad, with an average pore diameter of 56 Å.

An aerogel was prepared by removing the solvent from a gel prepared from **1** in toluene using supercritical carbon dioxide. Large pieces of the aerogel were opaque and white, but small pieces were transparent and appeared slightly orange when viewed through an optical microscope with transmitted light. Calcination of the aerogel at 500 °C for 2 h under flowing oxygen resulted in a material with a BET surface area of 564 $m^2\ g^{-1}$. The total pore volume of the calcined aerogel was 2.19 $cm^3\ g^{-1}$ and the average pore diameter was 155 Å.

The acid strengths of the $ZrSi_4O_{10}$ xerogel and aerogel calcined under O_2 at 500 °C for 2 h were estimated by contacting the solids with toluene solutions of various Hammett indicators.[10c] The strongest acid sites on the calcined xerogel were able to protonate benzalacetophenone ($pK_a = -5.6$) but not anthraquinone ($pK_a = -8.2$). The calcined aerogel contained acid sites strong enough to protonate dicinnamalacetone ($pK_a = -3.0$) but not benzalacetophenone ($pK_a = -5.6$). The materials prepared by the thermolysis of both **1** and **2** under oxygen at 500 °C also displayed acidic behavior. Both of these solids protonate dicinnamalacetone ($pK_a = -3.0$) but not benzalacetophenone ($pK_a = -5.6$).

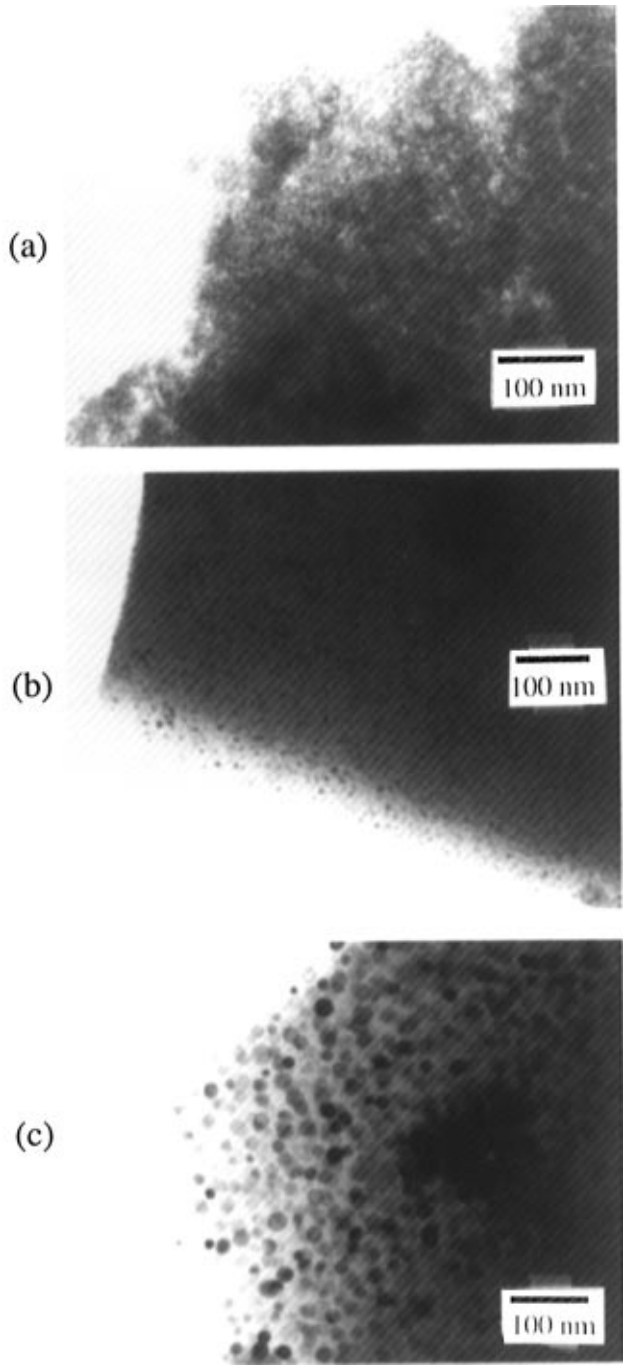

Figure 9. TEM photographs of xerogel derived from **1** after calcination under O_2 at (a) 900 °C, (b) 1200 °C, and (c) 1400 °C.

Solution Chemistry of Network Formation. The chemical changes associated with the thermal decomposition of **1** in solution were studied primarily by NMR spectroscopy. A toluene-d_8 solution of **1** containing a quantity of ferrocene standard was heated to 100 °C, and the course of the reaction was monitored by ^{1}H NMR spectroscopy. A plot of the disappearance of **1** and appearance of decomposition products (^{t}BuOH, $(^t$BuO$)_3$SiOH, and isobutene) as a function of time is given in Figure 11. Within the first 400 s of the thermolysis, 27% of **1** is consumed and small amounts of $(^t$BuO$)_3$SiOH and an unidentified Zr-OSi$(O^t$Bu$)_3$ complex giving rise to a singlet at δ 1.49 are formed (in a 1:3 integrated ratio). Further decomposition of the precursor then ceases temporarily. After an induction period of about 45 min, disappearance of **1** resumes

(26) Wies, Ch.; Meise-Gresch, K.; Müller-Warmuth, W.; Beier, W.; Göktas, A. A.; Frischat, G. H. *Phys. Chem. Glasses* **1990**, *31*, 138.

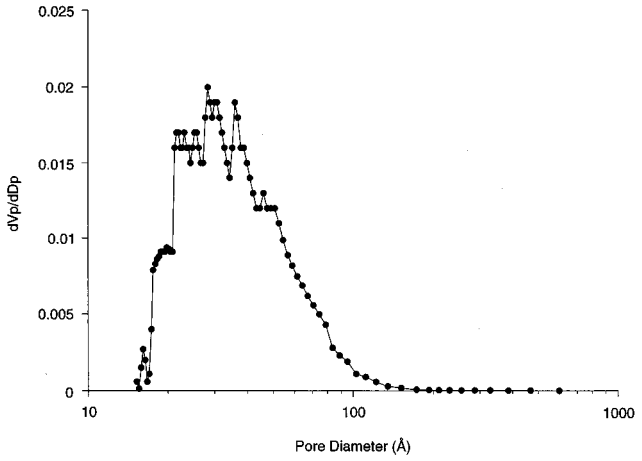

Figure 10. Pore size distribution for the xerogel prepared from **1**, after calcination at 500 °C under O_2 for 2 h.

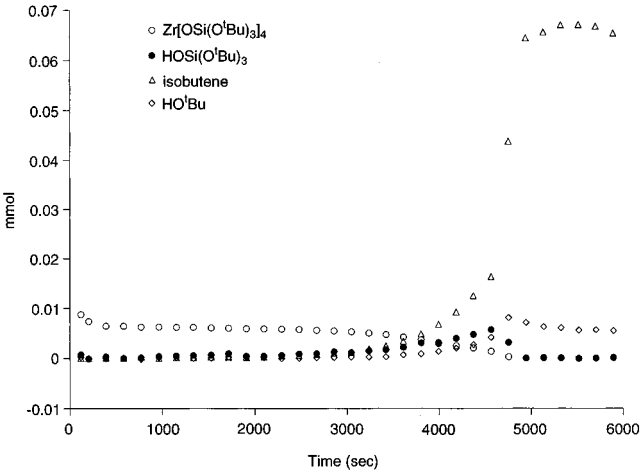

Figure 11. Concentration changes for **1**, $HOSi(O^tBu)_3$, ^tBuOH, and isobutene during the thermolysis of **1** in toluene-d_8 at 100 °C, as monitored by ^1H NMR spectroscopy.

and gives rise to a second unidentified zirconium complex and significant quantities of isobutene. As the concentration of **1** approaches zero, the $(^tBuO)_3SiOH$ in solution decomposes to isobutene and ^tBuOH. In the final stages of the conversion, *tert*-butyl alcohol is slowly dehydrated to isobutene. After all of **1** was consumed, a free-flowing sol existed, which was converted upon further thermolysis to a transparent, viscous gel.

The dehydration of *tert*-butyl alcohol suggested that the solution thermolysis may have an acid-catalyzed component. Support for this was obtained from the reaction of **1** with 2 equiv of trifluoromethane sulfonic acid in benzene-d_6, which was observed to rapidly produce a large amount of isobutene, along with much smaller amounts of ^tBuOH and $(^tBuO)_3SiOH$. Furthermore, heating **1** in benzene-d_6 in the presence of 0.1 equiv of 1,8-bis(dimethylamino)naphthalene (proton sponge) at 100 °C led only to minor decomposition of **1** after 5 d. This indicates that the decomposition of **1** is primarily Bronsted acid-catalyzed. Note that the gel formed from thermolysis of **1** efficiently catalyzes the dehydration of ^tBuOH and $(^tBuO)_3SiOH$ to isobutene, since pure ^tBuOH and $(^tBuO)_3SiOH$ are stable indefinitely at 100 °C.

Formation of $MO_2 \cdot 4SiO_2$ Thin Films. The high solubilities of compounds **1** and **2** in nonpolar solvents, and their facile, low-temperature eliminations of carbon, make them useful precursors for the fabrication of thin films. One percent solutions of compounds **1** and **2** in benzene and cyclopentanone, respectively, were spun onto quartz disks. The resulting precursor films were decomposed under oxygen at 400 °C for 1 h (heating rate 20 °C min^{-1}), giving thin films of the MSi_4O_{10} materials. SEM photographs of these films demonstrated that they are smooth and crack free, except in the vicinity of the film edge.

Discussion

The ceramic precursor molecules **1** and **2** are available in large quantities by simple synthetic procedures. Interestingly, these compounds crystallize as a mixture of two structural isomers. Coexistence of these isomers and the presence of the chelating η^2-$OSi(O^tBu)_3$ ligand in the 5-coordinate complexes imply that these compounds are weakly Lewis acidic. This is presumably why **1** is dimeric in benzene solution.

The oxygen-rich compounds **1** and **2** are excellent single-source precursors to homogeneous zirconia-silica and hafnia-silica materials. The ceramic conversions occur at low temperatures, give the theoretical yield for $MO_2 \cdot 4SiO_2$ compositions, and occur without the incorporation of carbon, which is a problematic feature often associated with molecular precursor routes to ceramic materials.[2a,27] Thus, the $Si-O^tBu$ groups behave as "masked" Si−OH groups which are converted by gentle heating of the precursor compound. These clean conversions may be attributed to the preexisting oxygen coordination environments for the Zr and Si atoms in the precursor molecules. For comparison, the related compounds containing just one Si−C bond, $M[OSiPh(O^tBu)_2]_4$ (**3** and **4**), are more thermally stable, as shown by their TGA traces, and reveal more episodic weight losses which occur over a wider temperature range.

Interestingly, the solid-state transformation of **1** to zirconia-silica produces an open, fibrous material, which appears surprisingly well ordered on the basis of TEM analysis (Figure 5a). As this material is taken to higher temperatures, the structure changes very little (by TEM analysis). Such open, three-dimensional structures are of interest as light-weight ceramics, catalyst supports, and membranes. Calcination to higher temperatures (900−1200 °C) results in a coarsening of the microskeletal structure to a vermicular-type architecture. This structure is quite stable and does not sinter to a dense, nonporous material until above 1200 °C. The mesoscopic order observed in the zirconia-silica material derived from **1** is interesting, and suggests the possibility that the directionality of the condensation process may be oriented to some degree by the crystalline lattice of the precursor compound.

In contrast, the solution-phase thermolysis of **1** produces a xerogel composed of small primary particles (≤∼5 nm). A similar texture has been observed for silica gels obtained by hydrolysis of $Si(OMe)_4$ in an organic solvent (dioxane).[28] The xerogel obtained from **1** in toluene exhibits an N_2-adsorption isotherm which is consistent with a broad pore size distribution and a high degree of textural mesoporosity.[29] Silica xerogels, obtained by a two-step method involving acid and base catalysis, have a similar pore size distribution and texture (by TEM).[29b] These xerogels possess high surface areas (∼700 m^2 g^{-1} at 200 °C) which approach values observed for aerogels. This may result from use of nonpolar solvents, which due to their low surface tension minimize collapse of the network pore structure

(27) Seyferth, D.; Wiseman, G. H.; Schwark, J. M.; Yu, Y.-F.; Poutasse, C. A. In *Inorganic and Organometallic Polymers*; Zeldin, M., Wynne, K. J., Allcock, H. R., Eds.; ACS Symposium Series 360; American Chemical Society: Washington, DC, 1988; p 143.

(28) Artaki, I.; Zerda, T. W.; Jonas, J. *J. Non-Cryst. Solids* **1986**, *81*, 381.

(29) (a) Sing, K. S. W.; Everett, D. H.; Haul, R. A. W.; Moscou, L.; Pierotti, R. A.; Rouquérol, J.; Siemieniewska, T. *Pure Appl. Chem.* **1985**, *57*, 603. (b) Reference 3a, Chapter 9.

Table 4. Comparison of Crystallization Behaviors for Various Precursors to $n ZrO_2$-$m SiO_2$[a]

preparation method	ref	1st *T* *t*−ZrO_2 obsvd (°C)	1st *T* *m*−ZrO_2 obsvd (°C)	1st *T* cristobalite obsvd (°C)
$Zr[OSi(O^tBu)_3]_4$ thermolysis under O_2	*b*	1200	1300	1500
xerogel derived from heating $Zr[OSi(O^tBu)_3]_4$ in toluene	*b*	1000	>1400	1400
$Zr(OAc)_4 + 2Si(OEt)_4$	39	1000	>1450	<1450
$ZrO(NO_3)_2 + 4Si(OEt)_4$	32	1000	1000	1000
$ZrCl_4 + 5Si(O^iPr)_4$	8	800	>1300	
$3Zr(O^iPr)_4 + 2Si(OEt)_4$	7	900	1200	1300

[a] In general, crystallization temperatures were determined by heating the samples to given temperatures (usually at ≥100° intervals), cooling back to room temperature, and then recording the XRD pattern. [b] This work.

during solvent evaporation.[3a] However, the mesoporosity observed for this material seems to be due to the packing of primary particles (see Figure 9a). In an attempt to obtain a material with even higher porosity, an aerogel was prepared by exchange of the solvent for supercritical carbon dioxide. This led to a surface area of 564 $m^2\ g^{-1}$, which is similar to that observed for the xerogel heated to the same temperature (500 °C; see Figure 6). However, the pore volume for the aerogel is about 3 times greater than that for the corresponding xerogel, presumably due to a looser packing of primary particles.

The crystallization behavior of zirconia-silica systems has been the subject of numerous investigations, since phase changes can dramatically influence the properties of these materials.[11,23,30−35] Usually, at temperatures ranging from 800 to 1200 °C, nanoparticles of tetragonal zirconia form.[16b,36] These particles are stable at room temperature, even though the monoclinic form is thermodynamically preferred at room temperature for pure, bulk samples. As the temperature is increased, the t-ZrO_2 particles grow until they eventually transform to m-ZrO_2 at a particle diameter ≥∼30 nm.[31] At higher temperatures (>1400−1500 °C), the crystallization of cristobalite and zircon ($ZrSiO_4$) may be observed.[37] The initial formation of t-ZrO_2 and the "delayed" transformation to m-ZrO_2 have been rationalized in terms of the surface and strain energies associated with zirconia nanoparticles, and to difficulties in nucleating the martensitic t → m transformation, which is mildly displacive (3−5% by volume). It is this volume change which prohibits high temperature use of pure zirconia in ceramic materials.[38] The presence of silica has been found to retard the crystallization of t-ZrO_2, and the t → m transformation.[36b] Clearly, the phase behavior of zirconia in these systems is dramatically influenced by matrix effects, crystallite sizes, and the silica/zirconia ratio.

Since zirconia crystallizations from well-mixed, amorphous ZrO_2−SiO_2 samples require considerable diffusion and grain growth, there is an apparent correlation between the homogeneity of the initial sample and the observed crystallization temperatures. Evidence for this is found, for example, in a decrease in the rate of grain growth for t-ZrO_2 with decreasing ZrO_2 concentrations.[36a] Thus, in well-mixed samples, the crystallizations occur at higher temperatures and such materials are more useful for high-temperature applications due to their greater resistance to the "thermal shock" associated with the t → m transformation. Table 4 compares the crystallization behavior for materials obtained from the molecular precursor **1** with those for sol-gel formulations that are reported to give homogeneous samples. The most meaningful comparisons are to ZrO_2−SiO_2 ratios close to that defined by the molecular formula of **1** (20% zirconia). From this data, it appears that the materials derived from **1** are characterized by relatively high-temperature crystallizations. The enhanced stabilization of the amorphous and tetragonal phases, relative to those derived from many sol-gel systems, implies that these single-source precursors initially produce homogeneous materials, and that subsequent crystallizations are to a large degree diffusion-controlled. These comparisons should be interpreted with caution, since the reported crystallization temperatures are in general only approximately determined. Also, it is likely that the crystallization of cristobalite plays a large role in the crystallization behavior for zirconia, since the cristobalite matrix should be more rigid than amorphous silica, and therefore greatly retard diffusion and inhibit the t → m transformation.[33] For example, a late crystallization of cristobalite may permit the diffusion and grain growth needed for the crystallization of m-ZrO_2.

The atmosphere under which **1** is thermolyzed has a relatively small effect upon the final particle size of the ZrO_2 crystallites after calcination to 1400 °C (Table 3). The volume fraction of the transformed m-ZrO_2 is also similar in samples calcined under oxygen and argon. The major difference between crystallizations under oxygen and argon is reflected in the temperature at which t-ZrO_2 is first detected by XRD. Under argon, t-ZrO_2 is observed at 1000 °C, whereas under oxygen it is not detected until 1200 °C. The lower crystallization temperature for t-ZrO_2 under argon can be attributed to oxygen deficiency in this black material, which is evidenced by an EPR signal at $g = 2.0025$. The sample does not become completely colorless until 1100 °C, indicating that oxygen deficiencies persist until this point. It has been shown that black, oxygen-deficient ZrO_2 powders crystallize to t-ZrO_2 at lower temperatures compared to the stoichiometric oxide.[40] The EPR signals in these materials have been attributed to electrons trapped in oxygen vacancies ($g = 2.003$), and it has been shown that such defects promote the crystallization of t-ZrO_2.[25]

Figures 4a and 7 show that the zirconia-silica xerogel from **1** forms t-ZrO_2 after heating to 1000 °C under O_2, whereas the material obtained by solid-state thermolysis of **1** does not begin to crystallize until 1200 °C. This may indicate that ZrO_2 is more homogeneously distributed in the material produced by

(30) Osendi, M. I.; Moya, J. S.; Serna, C. J.; Soria, J. *J. Am. Ceram. Soc.* **1985**, *68*, 135.
(31) (a) Garvie, R. C. *J. Phys. Chem.* **1965**, *69*, 1238. (b) Garvie, R. C. *J. Phys. Chem.* **1978**, *82*, 218.
(32) Nagarajan, V. S.; Rao, K. J. *J. Mater. Sci.* **1989**, *24*, 2140.
(33) (a) Lange, F. F. *J. Mater. Sci.* **1982**, *17*, 225. (b) Lange, F. F. *J. Mater. Sci.* **1982**, *17*, 235.
(34) Heuer, A. H.; Claussen, N.; Kriven, W. M.; Rühle, M. *J. Am. Ceram. Soc.* **1982**, *65*, 642.
(35) Skandan, G.; Hahn, H.; Roddy, M.; Cannon, W. R. *J. Am. Ceram. Soc.* **1994**, *77*, 1706.
(36) (a) Kamiya, K.; Mabe, S.; Yoko, T.; Tanaka, K. *J. Ceram. Soc. Jpn. Inter. Ed.* **1989**, *97*, 227. (b) Nogami, M.; Nagasaka, K.; Kadono, K.; Kishimoto, T. *J. Non-Cryst. Solids* **1988**, *100*, 298. (c) Low, I. M.; McPherson, R. *J. Mater. Sci.* **1989**, *24*, 1648.
(37) Kanno, Y. *J. Mater. Sci.* **1989**, *24*, 2415.
(38) Heuer, A. H.; Ruhle, M. In *Advances in Ceramics, Science and Technology of Zirconia*; Claussen, N., Ruhle, M., Heuer, A. H., Eds.; The American Ceramic Society: Columbus, OH, 1984; Vol. 12, p 1.
(39) Li, X.; Johnson, P. F. In *Better Ceramics Through Chemistry*; Zelinski, B. J. J., Brinker, C. J., Clark, D. E., Ulrich, D. R., Eds.; Mater. Res. Soc. Symp. Proc. Vol. 180; Materials Research Society: Pittsburgh, 1990; p 355.
(40) (a) Torralvo, M. J.; Alario, M. A.; Soria, J. *J. Catal.* **1984**, *86*, 473. (b) Sun, Y.; Sermon, P. A. *J. Mater. Chem.* **1996**, *6*, 1019.

Scheme 1

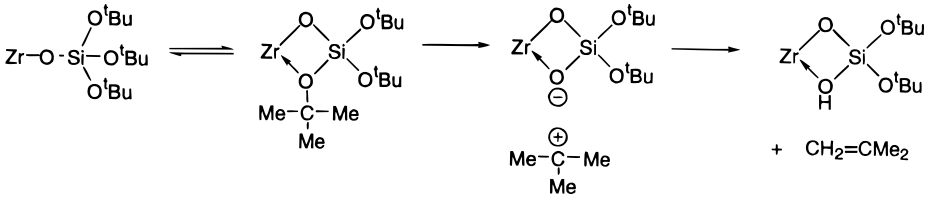

solid-state thermolysis. Calcination of the material prepared by the solid-state thermolysis of **1** to 1400 °C results in the transformation of 17 vol % ZrO_2 to the monoclinic phase. In contrast, no m-ZrO_2 is detected after calcination of the xerogel from **1** to 1400 °C. The stability of t-ZrO_2 in the latter sample may be attributed to the superior sintering behavior of the xerogel, which is composed of smaller primary particles with a high surface free energy. This promotes more efficient densification as the material is calcined. As a result, the xerogel forms a dense ceramic at 1200 °C, whereas the material from the solid-state decomposition does not sinter to a dense form until 1400 °C. Note also that cristobalite crystallizes somewhat earlier in this sample. Thus, the diffusion and grain growth required for producing m-ZrO_2 particles may be more inhibited in this material. The earlier formation of a dense matrix inhibits further grain growth of the ZrO_2 crystallites, resulting in a narrower crystallite size distribution in the xerogel derived ceramic (Figure 12).

The HfO_2·$4SiO_2$ system is also characterized by somewhat late crystallizations and a rather stable amorphous phase (Table 3). However, we observe that the transformation to m-HfO_2 at ∼1300 °C is far more extensive (∼50% of the crystallized hafnia at this point is in the mononclinic form). This probably reflects the greater thermodynamic stability of m-HfO_2 over t-HfO_2 at room temperature. For comparison, the t → m transformation temperatures for hafnia and zirconia are 1950 °C and 950 °C, respectively.

The solid-state ^{29}Si NMR spectra support the view that the zirconia-silica samples prepared by the solution route are well-mixed and contain significant quantities of Zr−O−Si linkages. Earlier studies have indicated that the peak centered at −110 ppm is due to $Si(OSi)_4$ (Q^4) sites, and that peaks observed at lower fields (−90 to −105 ppm) correspond to $Si(OSi)_{4-n}(OZr)_n$ entities (n = 1,2; designated as Q^3 and Q^2 sites, respectively).[7,8,26] This is supported by the ^{29}Si NMR spectrum for **1**, which contains a peak at −100.5 ppm. As can be seen in Figure 8, the sample taken to 600 °C contains a preponderance of Q^2 and Q^3 sites, and as the sample is heated to 1200 °C, considerable phase separation occurs to give mostly Q^4 sites.

Heterolinkages have been associated with acid sites in zirconia-silica materials.[11] For this reason, we have carried out preliminary investigations to characterize the acidity of materials obtained from molecular precursor **1**. From results with various Hammett indicators, we can estimate that the Hammett acidity function (H_o) of the strongest acid sites in the xerogel obtained from **1** is between −5.6 and −8.2. Since this method for estimating the acidity properties of a solid material is quite approximate, we are currently exploring alternative methods based on adsorption studies and acid-catalyzed reactions.

Relatively few mechanistic studies have addressed the pyrolytic transformation of metal alkoxide and metal siloxide complexes to oxide materials. However many investigations on potentially related processes involving the catalytic dehydration of alcohols by solid acids have been carried out.[41] Pioneering work by Bradley demonstrated that Zr(O-*tert*-amyl)$_4$ decomposes to ZrO_2 by an autocatalytic mechanism in the presence of water.[42] More recently, Chisholm has observed a similar process for $Mo_2(O^tBu)_6$ and $Al_2(O^tBu)_6$.[43] Sen and coworkers have identified complex homolytic and hydrogen-transfer schemes for the decompositions of titanium and cerium alkoxides.[44] The solid-state conversion of **1** to amorphous

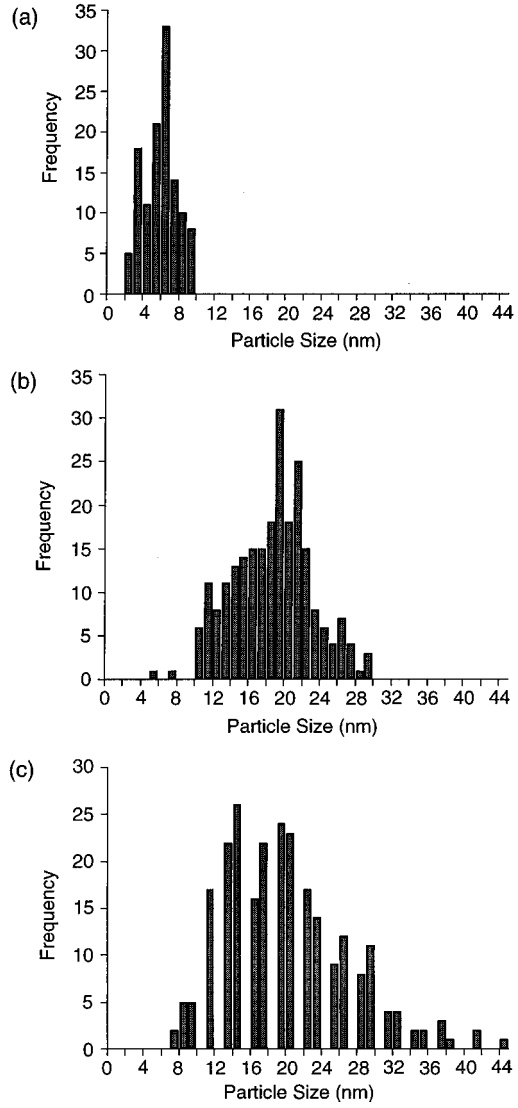

Figure 12. ZrO_2 crystallite size distribution measured from TEM micrographs for the (a) xerogel from **1** calcined to 1200 °C, (b) xerogel from **1** calcined to 1400 °C, and (c) product from the solid-state thermolysis of **1** at 1400 °C.

(41) (a) Noller, H.; Andréu, P.; Hunger, M. *Angew. Chem., Int. Ed. Engl.* **1971**, *10*, 172. (b) Knözinger, H. *Angew. Chem., Int. Ed. Engl.* **1968**, *7*, 791.

(42) (a) Bradley, D. C. *Chem. Rev.* **1989**, *89*, 1317. (b) Bradley, D. C.; Faktor, M. M. *Trans. Faraday Soc.* **1959**, *55*, 2117.

(43) Baxter, D. V.; Chisholm, M. H.; DiStasi, V. F.; Klang, J. A. *Chem. Mater.* **1991**, *3*, 221.

$ZrSi_4O_{10}$ is accompanied by the relatively clean elimination of 12 equiv of isobutene and 6 equiv of water. It is not known whether or not these represent the direct elimination products of thermolysis, since any *tert*-butyl alcohol that might form could be efficiently dehydrated, by the initially formed zirconia-silica material, to isobutene and water.[41,42] The mechanism of this conversion is somewhat obscure at this time, but we envision a process of the type shown in Scheme 1 (illustrated for an intramolecular version of the reaction). In fact the elimination of isobutene may occur by a more concerted process involving β-transfer of hydrogen to oxygen as the C−O bond is broken.[45] The heterolytic cleavage in Scheme 1 could, of course, be assisted by catalytic protonations at oxygen.

Conclusions

The thermolytic transformations of **1** and **2** to ceramic materials represent a novel synthetic pathway to zirconia- and hafnia-silica materials. These conversions provide theoretical yields for the final ceramics, which appear to possess homogeneous distributions of silicon and the transition metal in the oxide matrix. This is attributed to preservation of molecular-level homogeneity in the transition from precursor to ceramic material. The solid-state transformation of **1** gives relatively ordered, porous structures. The mechanism of this transformation is at present unclear, but this observation raises the interesting possibility that the regular array of the precursor's crystalline lattice may function as a scaffolding to orient the condensation reactions in particular directions. We are currently exploring this possibility with attempts to correlate structural features for various precursors with microstructural order in the corresponding ceramic material.

Solution-phase thermolysis of precursors such as **1** and **2** are potentially useful synthetic routes to oxide materials. These conversions represent an alternative to the sol-gel method and may offer certain advantages. First, this method seems to give homogeneous mixed-element oxides. Secondly, the condensation process is compatible with nonpolar (and polar) media. Therefore, it should be possible to prepare well-mixed, organic−inorganic composite materials via thermolysis of precursor compounds in the presence of organic substances. Finally, we anticipate that it should be possible to manipulate the stoichiometries of oxides via cothermolysis of precursor mixtures. This possibility is currently being explored.

Experimental Section

All manipulations were performed under an atmosphere of argon or nitrogen using standard Schlenk techniques and/or in a Vacuum Atmospheres dry box. NMR spectra were recorded on a Bruker AMX400 (at 400 (^{1}H), or 100 (^{13}C) MHz) or a GE QE-300 (at 300 (^{1}H), 75.5 (^{13}C), or 59.6 (^{29}Si) MHz) spectrometer. Infrared spectra were recorded on a Perkin Elmer 1330 spectrophotometer. The ^{29}Si MAS-NMR experiments were performed on a NT150 spectrometer (at 29.81 MHz) at the Colorado State University Regional NMR Center. Thermolyses were performed using a Lindberg 1700 °C or a Lindberg 1200 °C three-zone tube furnace. Heat treatments were carried out with flowing (100 cm^3 min^{-1}) argon (99.998%) or oxygen (99.6%). The heating rate was 10 °C min^{-1} to the specified temperature, which was typically maintained for 2 h. The samples were then cooled at a rate of 10 °C min^{-1}. Thermal analyses were performed on a Du Pont model 2000 thermal analysis system. Electron microscopy was performed on a Philips 301 TEM. Specific surface areas were measured using the BET method on a Quantachrome surface area analyzer. Multipoint surface area analyses were performed at Porous Materials, Inc., or Pacific Sorption Service. Powder X-ray diffraction was performed on a Siemens D5000 diffractometer. Solution molecular weights were obtained by the Singer method.[46] Dry, oxygen-free solvents were used throughout. Elemental analyses were performed at Mikro Analytisches Labor Pascher or Desert Analytics or at the College of Chemistry Microanalytical Facility. $LiNEt_2$ was freshly prepared from $HNEt_2$ and ^{n}BuLi. $ZrCl_4$ and $HfCl_4$ were purified by sublimation (180 to 200 °C at ∼10^{-3} Torr) before use. Modified preparations for the complexes $M(NEt_2)_4$ (M = Zr and Hf) were employed.[47]

Zr(NEt$_2$)$_4$. Diethyl ether (300 mL) was added slowly to a solid mixture of $LiNEt_2$ (4.06 g, 0.0515 mol) and $ZrCl_4$ (3.00 g, 0.0129 mol) cooled to −78 °C. The reaction mixture was slowly warmed to room temperature over 3 h and then stirred for 12 h. The slightly yellow ether solution was filtered. The remaining residue was extracted two times with 30 mL of pentane. The ether and pentane filtrates were combined, and the volatile material was removed under dynamic vacuum. The remaining viscous liquid was distilled under vacuum (∼0.001 Torr) at 100 °C to yield $Zr(NEt_2)_4$ (3.45 g, 71%). ^{1}H NMR (benzene-d_6, 22 °C): δ 1.17 (t, J = 7 Hz, 24 H) 3.34 (q, J = 7 Hz, 16 H).

Hf(NEt$_2$)$_4$. Diethyl ether (300 mL) was added slowly to a solid mixture of $LiNEt_2$ (5.91 g, 0.075 mol) and $HfCl_4$ (6.00 g, 0.019 mol) cooled to −78 °C. The reaction mixture was warmed to room temperature after 1 h and then refluxed for 1.5 h. The mixture was stirred at room temperature for an additional 3 h. The workup was similar to that for $Zr(NEt_2)_4$. Distillation under vacuum (∼0.001 Torr) at 90 °C yielded 6.55 g (75%) of $Hf(NEt_2)_4$. ^{1}H NMR (benzene-d_6, 22 °C): δ 1.14 (t, J = 7 Hz, 24 H) 3.35 (q, J = 7 Hz, 16 H).

Zr[OSi(O^{t}Bu)$_3$]$_4$ (1). A pentane solution (75 mL) of $(^t$BuO$)_3$SiOH (21.00 g, 0.0794 mol) was added to a stirred pentane solution (75 mL) of $Zr(NEt_2)_4$ (7.528 g, 0.0199 mol) which had been cooled to 0 °C with an ice bath. After 10 min, the ice bath was removed, and the reaction mixture was stirred for 6.5 h. The solvent was removed under reduced pressure, and the resulting solid was extracted into pentane (80 mL). Concentration and cooling (−40 °C) of this solution afforded 20.65 g of **1** as white crystals in 91% yield. Anal. Calcd for $C_{48}H_{108}O_{16}Si_4Zr$: C, 50.4; H, 9.50. Found: C, 50.5; H, 9.89. IR (CsI, Nujol, cm^{-1}): 1388 m, 1365 m, 1240 m, 1216 w sh, 1190 m, 1062 s, 1026 m sh, 980 w, 935 s, 830 m, 800 vw, 701 m, 640 br w, 635 w sh, 566 w, 505 w sh, 489 w, 466 w sh, 423 w, 371 w, 300 w. ^{1}H NMR (benzene-d_6, 22 °C): δ 1.52. ^{13}C{^{1}H} NMR (benzene-d_6, 22 °C): δ 32.18 (C*Me*$_3$), 72.59 (*C*Me$_3$). ^{29}Si NMR (benzene-d_6, 22 °C): δ −100.50 (s). Molecular weight in benzene: 2374 g mol^{-1}. Calculated for the dimer: 2290 g mol^{-1}.

Hf[OSi(O^{t}Bu)$_3$]$_4$ (2). This compound was synthesized in 94% yield by the method described for **1**. Anal. Calcd. for $C_{48}H_{108}HfO_{16}Si_4$: C, 46.79; H, 8.83. Found: C, 46.78; H, 8.93. IR (Nujol, CsI, cm^{-1}): 1385 m, 1363 m, 1240 m, 1215 w sh, 1190 m, 1062 s, 1026 m sh, 954 s, 830 m, 800 vw sh, 701 m, 640 br w, 567 br vw, 565 br vw, 505 w sh, 487 w, 467 br w sh, 424 w, 370 br w, 290 br w. ^{1}H NMR (benzene-d_6, 22 °C): δ 1.52. ^{13}C{^{1}H} NMR (benzene-d_6, 22 °C): δ 32.18 (C*Me*$_3$), 72.57 (*C*Me$_3$). ^{29}Si NMR (benzene-d_6, 22 °C): δ -97.06 (s). Molecular weight in benzene: 1049 g mol^{-1}. Calculated for the monomer: 1232 g mol^{-1}.

Zr[OSiPh(O^{t}Bu)$_2$]$_4$ (3) and Zr[OSiPh(O^{t}Bu)$_2$]$_4$·HNEt$_2$ (3·HNEt$_2$). To a solution of $Zr(NEt_2)_4$ (0.798 g, 2.08 mmol) in pentane (15 mL) was added $(^t$BuO$)_2$PhSiOH (2.232 g, 8.314 mmol) in pentane (35 mL). The solution was stirred for 45 min, and the volatile material was then removed under dynamic vacuum leaving a white solid which was kept under dynamic vacuum for 12 h. The resulting white solid was extracted into pentane (50 mL). Concentration to a saturated solution, and cooling to −35 °C, gave **3**·$HNEt_2$ (0.788 g) as an opaque white solid in 31% yield. A second crop was taken at −35 °C, yielding 0.334 g (14%) of base-free **3**. Anal. Calcd for $C_{60}H_{103}NO_{12}Si_4Zr$: C, 58.40; H 8.41; N 1.14. Found C, 58.27; H, 8.22; N, 0.96. ^{1}H NMR for **3**·$HNEt_2$ (benzene-d_6, 22 °C): δ 1.05 (t, J = 7.2 Hz, 6 H, NCH_2CH_3),

(44) (a) Stecher, H. A.; Sen, A.; Rheingold, A. L. *Inorg. Chem.* **1989**, *28*, 3280. (b) Nandi, M.; Rhubright, D.; Sen, A. *Inorg. Chem.* **1990**, *29*, 3065.

(45) (a) Budzichowski, T. A.; Chisholm, M. H.; Streib, W. E. *J. Am. Chem. Soc.* **1994**, *116*, 389. (b) Jeffries, P. M.; Dubois, L. H.; Girolami, G. S. *Chem. Mater.* **1992**, *4*, 1169.

(46) (a) Signer, R. *Leibigs Ann. Chem.* **1930**, *478*, 246. (b) Zoellner, R. W. *J. Chem. Educ.* **1990**, *67*, 714.

(47) Bradley, D. C.; Thomas, I. M. *J. Chem. Soc.* **1960**, 3857.

1.39 (s, 72 H, CMe_3), 2.83 (br s, 4 H, NCH_2CH_3), 7.21, 7.22, 7.23, 7.23 (m 12 H, Ph) 7.96, 7.98, 7.98, 7.99, 7.99, 8.00 (m, 8 H, Ph). IR (Nujol, CsI, cm^{-1}): 3225 w (NH), 3060 w, 3040 w, 1590 vw, 1428 m, 1386 m, 1362 s, 1302 vw, 1239 s, 1204 s sh, 1187 s sh, 1120 s, 1055 vs, 1023 s sh, 997 m, 925 vs, 824 m, 810 m, 740 m, 712 s, 700 s, 648 w, 538 w sh, 497 m sh, 474 m, 430 w, 361 w, 300 m. For **3**: Anal. Calcd for $C_{56}H_{92}O_{12}Si_4Zr$: C, 57.94; H, 7.99. Found C, 57.09; H, 7.86. ^{1}H NMR (benzene-d_6, 22 °C): δ 1.40 (s, 72 H, CMe_3), 7.21, 7.22, 7.23, 7.23 (m, 12 H, Ph), 7.96, 7.97, 7.98, 7.99 (m, 8 H, Ph). IR (Nujol, CsI, cm^{-1}): 3060 vw sh, 3040 vw, 1590 vw, 1428 m, 1387 m, 1362 s, 1240 m, 1202 m sh, 1188 s, 1122 s, 1055 vs, 1025 s sh, 998 m sh, 928 vs, 825 w, 810 w, 790 w, 712 s, 698 s, 648 w, 544 w br sh, 500 m, 466 m sh, 430 w sh, 362 w br, 295 w br.

Hf[OSiPh(O^{t}Bu)$_2$]$_4$ (4). To a solution of $Hf(NEt_2)_4$ (0.512 g, 1.10 mmol) in pentane (10 mL) was added (^{t}BuO)$_2$PhSiOH (1.177 g, 4.384 mmol) in pentane (10 mL). The solution was stirred for 50 min and the volatile material was then removed under dynamic vacuum. The remaining white solid was kept under dynamic vacuum for 12 h and then extracted into pentane (20 mL). Concentration and cooling (−78 °C) of the pentane solution afforded **4** (0.934 g, 68%) as a white solid. Anal. Calcd. for $C_{56}H_{92}HfO_{12}Si_4$: C, 53.89; H, 7.43. Found C, 54.25; H, 7.72. ^{1}H NMR (benzene-d_6, 22 °C): δ 1.40 (s, 72 H, CMe_3), 7.20, 7.21, 7.22, 7.23 (m, 12 H, Ph), 7.96, 7.97, 7.99 (m, 8 H, Ph). IR (Nujol, CsI, cm^{-1}): 3055 w, 3035 vw, 1586 w, 1425 m, 1383 m, 1360 s, 1238 m, 1200 m sh, 1184 m, 1120 m, 1055 s br, 1021 m sh, 992 m, 945 s br, 822 w, 808 w, 738 m, 710 m, 696 m, 644 w br, 586 w sh, 494 m, 465 w sh, 427 vw sh, 360 vw, 288 w.

Gelation of 1 in Toluene and Ceramic Conversion to ZrO_2·4SiO_2. A toluene solution (10 mL) of compound **1** (1.5 g) was sealed in a 100 mL pyrex tube. The tube was placed in an oven (140 °C) for 48 h. The solid, wet gel was removed and air-dried for 5 d to form a xerogel. The hard xerogel was then ground to a fine powder, which was heated to 100 °C for 3 h under vacuum. Calcination of the gel was performed in a tube furnace under flowing oxygen. The temperature was ramped at a rate of 10 °C min^{-1} to the desired value, and maintained for 2 h.

Solution Thermolysis of 1 in Toluene-d_8. To compound **1** (15.6 mg, 0.014 mmol) and ferrocene (6.6 mg, 0.036 mmol) in an NMR tube was added 0.88 mL of toluene-d_8. The tube was sealed and placed in an NMR probe preheated to 100 °C. The reaction was followed to completion by periodically recording the molar amounts of reactants and products.

Supercritical Drying of the Gel Obtained from 1 in Toluene. The transparent, wet gel, prepared as described above, was dried using supercritical carbon dioxide in a 300 mL Polaron Critial Point Dryer. The majority of the toluene was replaced by flowing liquid CO_2 (5 °C, 850 psi) over a 3 h period. During this process, the gel changed from colorless and transparent to opaque and white. The system was maintained under these conditions overnight to ensure complete diffusion of toluene from within the gel. After an additional 1 h of liquid CO_2 purging, the CO_2 inlet was closed and the temperature of the vessel was raised to 45 °C. The CO_2 was vented to maintain a pressure of 1350−1450 psi. After maintaining these conditions for 1 h, the system was vented to ambient pressure over 45 min, and then the vessel was opened and the aerogel was removed.

Estimation of the Acid Strength for Solid ZrO_2·4SiO_2 Samples. The acid strength of the ZrO_2·4SiO_2 materials was measured on samples which were calcined under O_2 at 500 °C for 2 h. After calcination, the samples were contacted with anhydrous toluene solutions of a Hammett indicator. The appearance of the acid color of the Hammett indicator implies that the gel has acid sites whose Hammett acidity function (H_o) is equal to or less than the pK_a value of the indicator. The following indicators were used methyl red (pK_a = +4.8), 4-(phenylazo)diphenylamine (pK_a = +1.5), dicinnamalacetone (pK_a = −3.0), benzalacetophenone (pK_a = −5.6), and anthraquinone (pK_a = −8.2).

Thin-Film Formation from 1. (Representative procedure) Compound **1** (19 mg) was dissolved in 1.845 g of benzene. Under nitrogen, a 1 in. diameter quartz disk was saturated with the solution. The disk and solution were spun at ∼1000 RPM for 1 min to form a precursor film of **1**. This film was then pyrolyzed at 20 °C min^{-1} to 400 °C (1 h at 400 °C) under oxygen.

Crystallographic Structure Determinations. Crystallographic data are given in the Supporting Information. Crystals of **1** were grown from a concentrated pentane solution at −40 °C. At room temperature the crystals fracture within 1 h. A colorless blocky crystal of dimensions 0.25 × 0.20 × 0.10 mm was mounted on a glass fiber using Paratone N hydrocarbon oil. The mounted crystal was placed under a cold stream of nitrogen on the diffractometer within 20 min of removing the crystals from the freezer. Data was collected using a Siemens SMART diffractometer with a CCD area detector. A preliminary orientation matrix and unit cell parameters were determined by collecting 60 10-s frames, followed by spot integration and least-squares refinement. A volume including one unique quadrant of data was collected using ω scans of 0.3° and a collection time of 10 s per frame. Frame data was integrated (*XY* spot spread = 1.16°; *Z* spot spread = 0.40°) using SAINT. The data were corrected for Lorentz and polarization effects. An absorption correction was performed using XPREP (μR = 0.05, T_{max} = 0.94, T_{min} = 0.83). The 32 947 integrated reflections were averaged in point group 2/*m* to give 14 080 unique reflections (R_{int} = 0.093). Of these, 6137 reflections were considered observed ($I > 3.00\sigma(I)$). No decay correction was necessary. Inspection of the systematic absences uniquely defined the space group as *C*2/*c*. The structure was solved using direct methods (SAPI91), expanded using Fourier techniques (DIRDIF92), and refined by full-matrix least-squares methods using teXsan software. The non-hydrogen atoms were refined anisotropically. The hydrogen atoms were included at calculated positions but not refined. The number of variable parameters was 933 giving a data:parameter ratio of 6.53. The maximum and minimum peaks on the final difference Fourier map corresponded to 0.80 and −0.92 e$^-$ Å^{-3}: R = 0.065, R_w = 0.066, GOF = 1.61.

Crystals of **2** were grown from a concentrated toluene solution at −40 °C. A colorless blocky crystal of dimensions 0.38 × 0.27 × 0.25 mm was mounted on a glass fiber using Paratone N hydrocarbon oil. Data was collected as above. Frame data was integrated (*XY* spot spread = 0.9°; *Z* spot spread = 0.40°) using SAINT. The data were corrected for Lorentz and polarization effects. An absorption correction was not performed. The 34 231 integrated reflections were averaged in point group 2/m to give 13 920 unique reflections (R_{int} = 0.054). Of these, 10 595 reflections were considered observed ($I > 3.00\sigma(I)$). No decay correction was necessary. Inspection of the systematic absences uniquely defined the space group as *C*2/*c*. The structure was solved using direct methods (SIR92), and refined by full matrix least-squares methods using teXsan software. Two oxygen atoms which were modeled as disordered over two sites, O(23)/O(24) and O(25)/O(26), were refined isotropically. The remaining non-hydrogen atoms were refined anisotropically. The hydrogen atoms were included at calculated positions but not refined. The number of variable parameters was 931 giving a data:parameter ratio of 11.38. The maximum and minimum peaks on the final difference Fourier map corresponded to 1.03 and −1.66 e$^-$ Å^{-3}: R = 0.038, R_w = 0.050, GOF = 1.75.

Acknowledgment. This work was supported by the Director, Office of Energy Research, Office of Basic Energy Sciences, Chemical Sciences Division, of the U.S. Department of Energy under Contract No. DE-AC03-76SF00098. We also thank Drs. Arlon Hunt and Michael Ayers for help in preparing the aerogel samples.

Supporting Information Available: Tables of crystal, data collection, and refinement parameters, bond distances and angles, and anisotropic displacement parameters (31 pages). See any current masthead page for ordering and Internet access instructions.

JA971405V